

Pyroelectric energy conversion using $\text{Ba}_{0.85}\text{Sr}_{0.15}\text{Zr}_{0.1}\text{Ti}_{0.9}\text{O}_3$ ceramics and its cement-based composites

Journal of Intelligent Material Systems
and Structures

2019, Vol. 30(6) 869–877

© The Author(s) 2019

Article reuse guidelines:

sagepub.com/journals-permissions

DOI: 10.1177/1045389X19828491

journals.sagepub.com/home/jim



Anuruddh Kumar¹, Sidhant Kumar¹, Satyanarayan Patel², Moolchand Sharma¹, Puneet Azad³, Rahul Vaish¹ , Rajeev Kumar¹ and KS Srikanth¹

Abstract

In this article, we focus on cement-binded $\text{Ba}_{0.85}\text{Sr}_{0.15}\text{Zr}_{0.1}\text{Ti}_{0.9}\text{O}_3$ ceramics for pyroelectric applications. It was prepared with the $\text{Ba}_{0.85}\text{Sr}_{0.15}\text{Zr}_{0.1}\text{Ti}_{0.9}\text{O}_3$ -to-cement ratios of 85%:15% and 80%:20% by weight. In order to improve the effectiveness of thermal-to-electric energy conversion, the synchronized switch harvesting on inductor technique is experimentally tested on cement composites. Our experimental findings reveal that this concept based on synchronized switch harvesting on inductor can significantly increase the amount of power extracted from pyroelectric materials. Furthermore, the optimized power across 15% and 20% cement composites were found to be 7.2 and 6 nW, respectively, in series synchronized switch harvesting on inductor and 8.5 and 7 nW, respectively, in parallel synchronized switch harvesting on inductor. These values are significantly higher when compared with non-switched circuit for pyroelectric applications. Although, from the obtained results for the prepared composites, the power output is less when compared with pure $\text{Ba}_{0.85}\text{Sr}_{0.15}\text{Zr}_{0.1}\text{Ti}_{0.9}\text{O}_3$, they have some advantages: these composites can be made without any sintering process and are compatible for structural applications.

Keywords

Pyroelectric, cement composites, dielectric, ferroelectric

1. Introduction

The pyroelectric materials are well known for their unique thermoelectric conversion ability (Lang, 2005; Lau et al., 2008; Li et al., 2013; Yao et al., 2012). These materials show high sensitivity toward temporal temperature change and have garnered researchers' attention because of their huge potential in market for sensors, detectors, and thermal imaging applications (Bauer and Ploss, 1990; Lau et al., 2008; Whatmore, 1986). The thrust for looking for low-cost materials for efficient usage of these materials is a subject of interest among the researchers. A large number of ceramics is already explored by researchers across the globe for various pyroelectric applications (Lang et al., 2006; Patel et al., 2015a; Sasaki et al., 1999). With a view to derive the best performance out of pyroelectric materials, there should be optimum tradeoff between dielectric constant, dielectric loss, pyroelectric coefficient, and specific heat as these properties have a direct impact on pyroelectric figure of merit (FOM) which is a method of quantifying the materials' performance for pyroelectric device applications (Patel et al., 2015b; Zhang et al., 2009). An improvement in FOMs can be achieved by

either degrading the dielectric constant or enhancing the pyroelectric coefficient which can be accomplished by either physical or chemical modifications (Patel et al., 2015b, 2016; Patel and Vaish, 2016). The fabrication of composites is another technique to tune all physical properties as per requirements. Keeping the composites' route in mind, several academic groups/researchers have explored the polymer matrix composites in the past for various dielectric applications (Clegg et al., 1997; Dietze et al., 2007; Furukawa et al., 1976). Another handy technique to improve the pyroelectric performance of materials is by inducing pores (porous ceramics) where density and dielectric constant decrease

¹School of Engineering, Indian Institute of Technology, Mandi, Himachal Pradesh, India

²Institute of Materials Science, Technische Universität Darmstadt, Darmstadt, Germany

³Department of Electronics & Communication Engineering, Maharaja Surajmal Institute of Technology, New Delhi, India

Corresponding author:

Rahul Vaish, School of Engineering, Indian Institute of Technology, Mandi 175 005, Himachal Pradesh, India.

Email: rahul@iitmandi.ac.in

drastically due to the incorporation of pores (Roscoe et al., 2015; Shaw et al., 2007; Zhang et al., 2010) which are desirable for pyroelectric applications. Generally, introduction of pores is done by some pore-forming agents like poly-methyl methacrylate (PMMA) and burning them out during the sintering process so as to leave pores in the material which can help in tuning the pyroelectric performance of materials. However, fabricating porous ceramics is another challenging task.

In this direction, cement-binded pyroelectric composites have many advantages, for example, ease of fabrication and promising in real-time structural health monitoring sensors, as they are compatible with cement structures (Dong et al., 2015; Lu et al., 2015). Although a number of attempts have been made to explore piezoelectric signals in cement-based composites (Gong et al., 2009; Li et al., 2009), there is very little work done on exploring cement-binded pyroelectric composites for pyroelectric applications. In one such study, the pyroelectric coefficient of steel fiber cement paste ($61 \times 10^{-9} \text{ C/m}^2 \text{ K}$) and carbon fiber cement paste ($3.5 \times 10^{-9} \text{ C/m}^2 \text{ K}$) is reported (Wen and Chung, 2003). These values are very low and need to be improved. In order to further improve the functionality of cement-based materials for pyroelectric applications, we have synthesized cement-binded $\text{Ba}_{0.85}\text{Sr}_{0.15}\text{Zr}_{0.1}\text{Ti}_{0.9}\text{O}_3$ (BSZTO) ceramics. The BSZTO was selected in this investigation as it exhibits promising pyroelectric properties (Patel et al., 2016; Patel and Vaish, 2016). It has a pyroelectric coefficient of $25 \times 10^{-4} \text{ C/m}^2 \text{ K}$ at room temperature which is almost nine times more than that of the well-known pyroelectric material triglycine sulfide (TGS) with a pyroelectric coefficient of $2.8 \times 10^{-4} \text{ C/m}^2 \text{ K}$ (Patel et al., 2016). This composition also exhibits substantial FOMs at room temperature over other materials as reported by Patel et al. (2016). Such a large-scale investigation suggests that it could be a strong contender for many commercial pyroelectric applications.

Therefore, this article deals with cement-binded BSZTO ceramics as a potential material for pyroelectric applications. The last section of this article presents the interface of synchronized switch harvesting on inductor (SSHI) for enhancing the power output across the pyroelectric element. SSHI is a non-linear approach of enhancing the voltage generated by different sources and has been extensively applied in energy harvesting (Chen et al., 2012; Cheng et al., 2017; Lefeuvre et al., 2009; Shu et al., 2007; Wu et al., 2017; Xi et al., 2017; Zi et al., 2016). The main advantages of such circuits are low power dissipation and increased efficiency. The inductor present in the circuit helps flip the voltage of the internal capacitance of the material/source used for harvesting energy with the help of triggering of a switch at suitable intervals. Thus, the presence of an inductor helps in boosting the overall power as compared to

non-switched circuits which is also discussed in this article.

2. Material synthesis and characterization

A conventional solid-state fabrication route was employed to prepare BSZTO ceramics. Reagent-grade (with purity $> 98.5\%$) powders of BaCO_3 , SrCO_3 , ZrO_2 , and TiO_2 were used as the starting precursors. Stoichiometric amounts of powders were mixed and ball milled using acetone as the wetting agent to attain physical homogeneity. The mixture was then calcined at 1350°C for 6 h after drying. The resultant mixture was compressed under a uniaxial pressure of 6 ton/cm^2 into pellets of $12 \text{ mm} \times 1 \text{ mm}$ (diameter \times thickness). Then the pellets were sintered by a conventional technique at 1400°C for 6 h. X-ray diffraction technique (Rigaku Smart Lab, Tokyo, Japan) employing $\text{CuK}\alpha$ radiation was performed to confirm the formation of a single phase. In order to prepare BSZTO–cement composites of varying compositions (15% and 20% cement by weight), the calcined powder was thoroughly mixed with ordinary Portland cement. Addition of water to the mixture according to certain water–cement ratio was done prior to pouring into the mold. The prepared mold specimens were cured for 28 days in water to obtain sufficient stiffness. Following this, the cement specimens were polished to obtain disk shapes with 12 mm diameter and 1 mm thickness. Scanning electron microscopy (SEM; FEI Nova NanoSEM 450 (Field Electron and Ion Company, FEI); Hillsboro, OR, USA) was used to study the morphology of the samples under consideration. Archimedes' principle was employed to determine the density of these samples. The dielectric properties of the composites were measured using an impedance analyzer at a heating rate of $1^\circ\text{C}/\text{min}$ (Agilent E4990A; Agilent Technologies Inc., Santa Clara, CA, USA). The samples were subsequently poled in a 3 kV/mm electric field for 2 h at 45°C in silicon oil in order to measure pyroelectric properties.

2.1. Methodology

In order to explore the investigated materials for pyroelectric applications, the poled sample was alternatively placed in front of hot and cold air for continuous temperature measurements for a fixed time interval as shown in Figure 1. It shows the internal electrical circuit for the pyroelectric element, where C_p and R_p are the material capacitance and resistance, respectively, and I_p denotes the pyroelectric current. Figure 2(a) presents the non-switched circuit which connects the pyroelectric element directly across load R_L . Now, according to Kirchhoff's current law as shown in equation (1), the quantity of current (I_p) which is produced due to

temperature gradient is the sum of current passing through material capacitance (C_p), material resistance (R_p), and load resistance (R_L) yielding

$$C_p \frac{dV_p}{dt} + \frac{V_p}{R_p} + \frac{V_p}{R_L} = I_p \quad (1)$$

Therefore, voltage V_p across the pyroelectric element is shown in equation (2)

$$V_p(t) = e^{c_p \left(\frac{-t}{k_p + k_L} \right)} + \frac{I_p}{C_p} \quad (2)$$

Since the voltage across load is the same as pyro-voltage, the average power (P) dissipated across the load resistance is calculated as shown in equation (3)

$$P = \frac{V_p^2}{R_L} \quad (3)$$

The SSHI technique is a non-linear approach in which an inductor stores the magnetic energy temporarily and is one of the common techniques in buck-boost converters also which exploits the feature of the inductor to store energy. The only limitation with such a design in which inductors are used to boost power is the losses in the circuit due to switch resistance and windings of the inductors. However, such losses are insignificant in comparison to the boosted power.

Figure 2(b) presents a parallel SSHI circuit in which a switching device consists of cascaded combination of an inductor and an electronic switch which are placed in parallel with a pyroelectric element. The synchronized switch harvesting principle works on the basis of synchronization between charge extraction and temperature gradient through an inductor by adding non-linear processing of the pyroelectric voltage with the help of an electronic switching device connected to the pyroelectric element (Guyomar et al., 2008; Lien et al., 2010). One of the important characteristics of this technique is that the pyroelectric element remains in open circuit condition for most of the time except when the triggering of switch takes place at the peak of pyroelectric voltage resulted from heating and cooling where LC_p oscillations take place with frequency (f) as denoted by equation (4)

$$f = \frac{1}{2\pi\sqrt{LC_p}} \quad (4)$$

where L is the inductor and C_p is the internal capacitance of the pyroelectric material. The inductor is connected either in parallel or in series to the pyroelectric material with a switching device controlled by a logic circuit using a metal oxide semiconductor field effect transistor (MOSFET). The control unit is assumed to turn on and off the MOSFET transistor at the

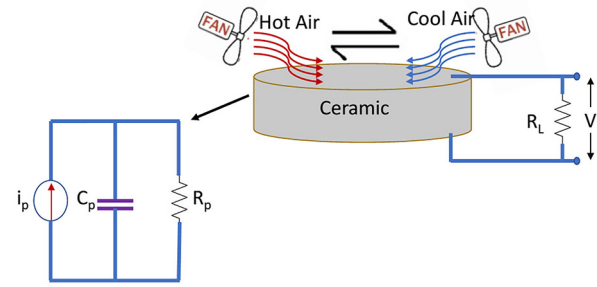


Figure 1. Schematic of the experimental set-up for pyroelectric signal generation on exposure to heating-cooling source and the inset shows internal electrical circuit of pyroelectric element.

switching frequency. One of the prime advantages of using MOSFET as a switch is their low power requirement and low switching time.

A constant time period of the heating and cooling cycle is maintained across the pyroelectric element such that the switch is triggered at each temperature extremum for a brief time period of $\pi\sqrt{LC_p}$ (Guyomar and Lallart, 2011; Lallart, 2017). During these triggering times, an electrical oscillation corresponds to L and C_p is established where an oscillating discharge of the pyroelectric voltage across capacitor C_p occurs through the inductor L which leads to inversion and enhancement of voltage across capacitor C_p as compared to non-switched interface (Lefeuvre et al., 2006). However, this inversion is not perfect due to internal losses of circuit and is given by coefficient γ as shown in equation (5) which represents the ratio of voltage after switching to voltage before closing. It is related to the electrical quality factor Q which represents the ratio of the stored energy to the dissipated energy (equation (6))

$$\gamma = e^{\frac{-\pi}{2Q}} \quad (5)$$

$$Q = \frac{1}{r} \sqrt{\frac{L}{C_p}} \quad (6)$$

where r represents the inductor losses in the circuit. This concept is explored in this article and the two techniques are differentiated to show their importance.

With Kirchhoff's current law, when the switch is closed as shown in Figure 1, we have

$$I_p = C_p \frac{dV_{ps}}{dt} + i_1 + \frac{V_{ps}}{R_L} \quad (7)$$

and

$$V_{ps} = L \frac{di_1}{dt} \quad (8)$$

where V_{ps} is the root mean square (RMS) voltage across the pyroelectric material after the switching process,

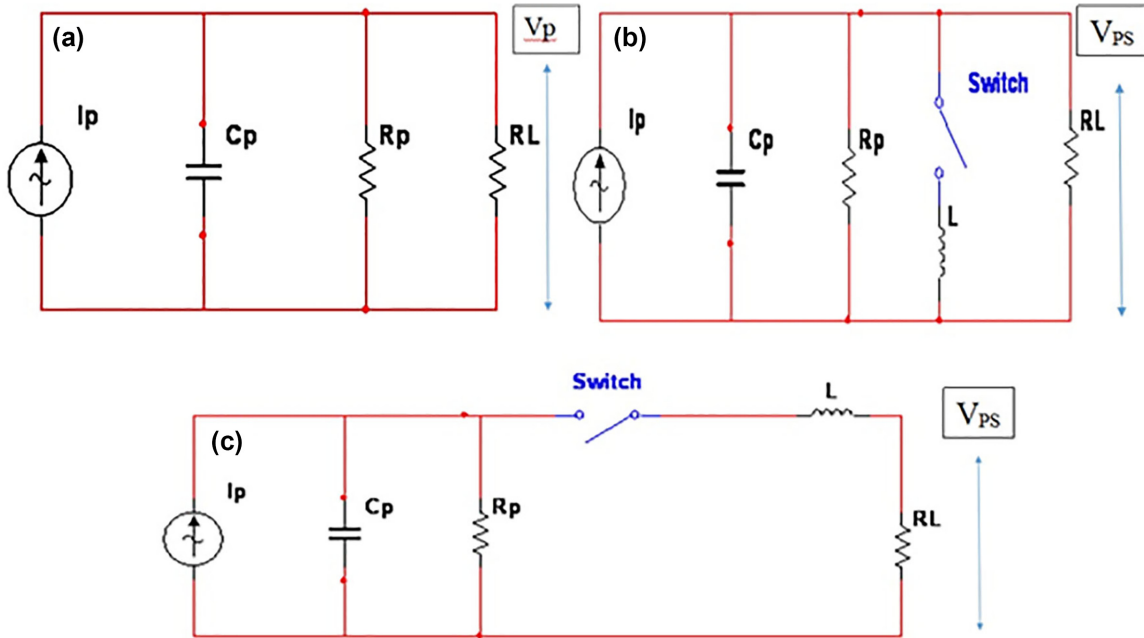


Figure 2. Schematic of (a) non-switched circuit, (b) parallel SSHI, and (c) series SSHI.

which is used to calculate power across different load resistances (R_L).

Now, we explore the series SSHI technique, the operation of which is similar to that of parallel SSHI. However, the electronic switching device consisting of an inductor and an electronic switch is connected in series as shown in Figure 2(c).

3. Results and discussion

The X-ray diffraction (XRD) pattern of the BSZTO ceramic confirms the formation of a single phase as shown in Figure 3(a). Figure 3(b(I)) shows the SEM micrograph recorded on the as-sintered surface of pure BSZTO ceramic. The sample exhibits good densification, with well-interconnected grains and without any major pores, having a bimodal grain size distribution (larger grains coexist with small grains). Furthermore, the density of the sintered sample was estimated using Archimedes' principle and found to be $\sim 95\%$ of the theoretical density, confirming the highly dense structure due to closely packed grains. The SEM micrographs of cement-binded composites with varying compositions (15% and 20%) are displayed in Figure 3(b(II)) and (b(III)), respectively. Microstructural observation demonstrates that the porosity tends to increase by increasing the content of cement which is consistent with the measured density of the samples.

Figure 4 presents the dielectric constant (ϵ_r) and dielectric loss ($\tan \delta$) of the understudied compositions. In this direction, the dielectric constant and loss are compared at a fixed frequency of 1 kHz for cement

compositions in Figure 4(a). It is evident from Figure 4(a) that the dielectric constant decreases with cement addition and found to be 114 and 76 for the 15% and 20% cement samples, respectively. The ϵ_r value measured at a constant frequency for the cement composites decreased with an increasing porosity (with cement content) due to the volume fraction effect which resulted in reduced density and can be explained based on the dominating effect of the passive phase (pores) over the active phase (BSZTO) of the material (Zhang et al., 2007). Moreover, we observed no shift in phase transition temperature (Curie temperature) at all with cement addition compared with pure BSZTO ceramic, the dielectric plots of which are shown in Figure 4(b). The dielectric constant is manifolds smaller for cement composites when compared with pure BSZTO ceramic. It is to note that the dielectric constant of the cement composite is not varied linearly with composition. It could be due to the change in microstructure with the addition of BSZTO. There is a significant effect of interfacial polarization which contributes to the non-monotonous dielectric behavior. In order to further understand the dielectric behavior of the understudied composites, researchers have proposed different types of models to describe the dielectric, piezoelectric, and pyroelectric properties of 0–3 composites which are based on mixture rules, such as those derived by Jayasundere and Smith (1993) as follows:

$$\epsilon = \frac{\epsilon_1 v_1 + \epsilon_2 v_2 [3\epsilon_1 / (\epsilon_2 + 2\epsilon_1)] [1 + 3v_2(\epsilon_2 - \epsilon_1) / (\epsilon_2 + 2\epsilon_1)]}{v_1 + v_2 [3\epsilon_1 / (\epsilon_2 + 2\epsilon_1)] [1 + 3v_2(\epsilon_2 - \epsilon_1) / (\epsilon_2 + 2\epsilon_1)]} \quad (9)$$

It describes the dielectric constant of a two-phase composite, where ϵ_1 , ϵ_2 , and ϵ are the dielectric constants of the matrix, inclusions, and composite, respectively, and v_1 and v_2 represent the volume fraction of the matrix and inclusions, respectively.

Based on the exciting model, we calculate the dielectric constant for the 15% and 20% cement composites. The values of dielectric constant obtained for the 15% and 20% cement composites are 40 and 26, respectively. However, the corresponding experimentally observed values are 95 and 60. It is clear that the composites (rule of mixture) method could not provide a good agreement with the measured ϵ_r , because it is also influenced by the particle/grain size (Figure 3), porosity of material, mixing, and connectivity (1–3, 0–3). Further detailed discussion on the effect of cement incorporation on the dielectric properties is discussed in Srikanth et al. (2018) and Xin et al. (2007). This decrease in the dielectric constant advantages immediate benefits in switching the pyroelectric FOMs (Liu et al., 2015; Roscow et al., 2015; Sun et al., 2014; Yu et al., 2012). In this regard, there are a couple of FOMs derived for pyroelectric materials for various applications (Liu et al., 2015; Roscow et al., 2015; Sun et al., 2014; Yu et al., 2012). In addition, the dielectric loss ($\tan \delta$) of the cement composites was found to increase (with an increase in cement content) as shown in Figure 4(a). Such a discrepancy can also be rationalized by

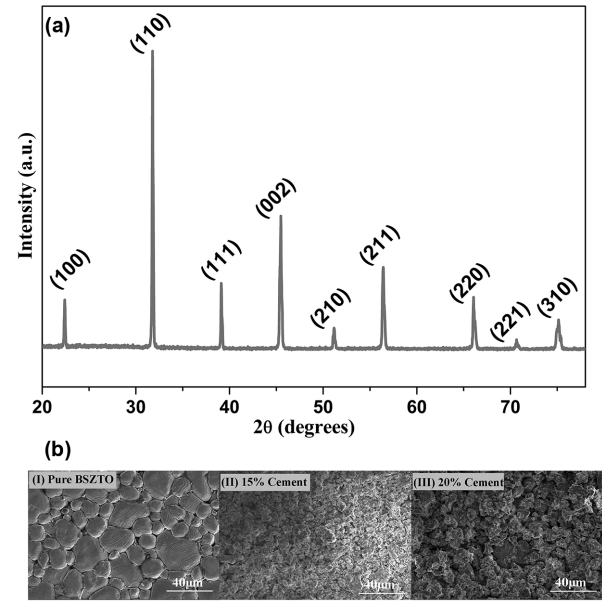


Figure 3. (a) X-ray diffraction pattern of the sintered BSZTO ceramic and (b) SEM micrographs of (I) sintered BSZTO, (II) 85% BSZTO–15% cement composite, and (III) 80% BSZTO–20% cement composites.

considering the porous microstructure of the samples. $\tan \delta$ also exhibits a well-defined peak at the transition temperature. It is interesting to note that the value of

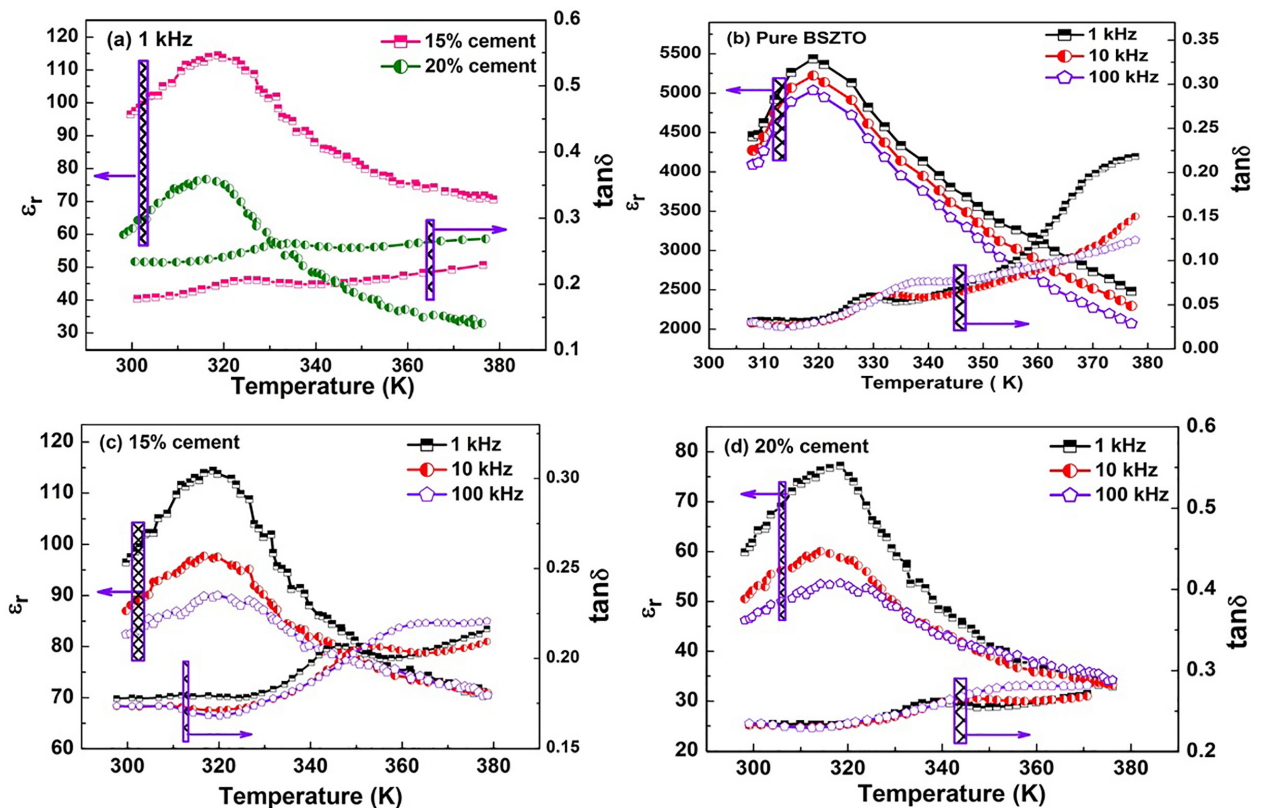


Figure 4. Temperature dependence of the dielectric constant (ϵ_r) and loss ($\tan \delta$) for (a) comparison at 1 kHz, (b) pure BSZTO, (c) 15% cement sample, and (d) 20% cement sample at different frequencies.

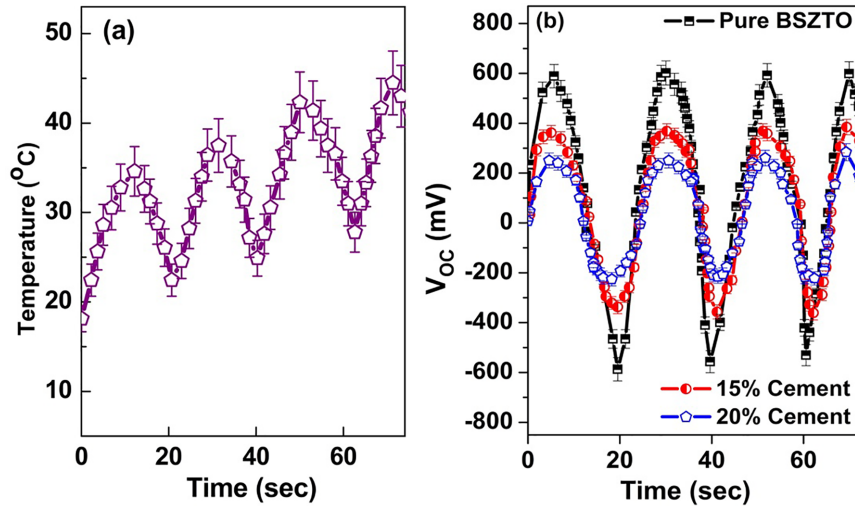


Figure 5. (a) Temperature profile near the pyroelectric material surface and (b) plots of open circuit voltage versus time for all the compositions.

$\tan \delta$ increased marginally in cement-based composites when compared with pure BSZTO. The measured capacitance is 4.4 nF, 96 pF, and 60 pF (at room temperature and 1 kHz), and the corresponding ϵ_r values are ~ 4400 , 96, and 90 for BSZTO ceramics and 15% and 20% cement composites, respectively.

Figure 5(a) presents the thermal gradient cycle in which the temperature increases from its starting value of room temperature and goes up to 45°C at a given cycle frequency (0.05 Hz) which is essential to have a temperature gradient and to have a continuous electrical signal from the pyroelectric material due to electrical displacement of dipoles, which leads to the open circuit voltages of 600, 360, and 250 mV in pure BSZTO and 15% and 20% cement composites, respectively, as shown in Figure 5(b). The pyroelectric coefficients of all the three samples can be measured by Byer–Roundy methods. However, in this study, voltage (V) is measured across the resistance ($R = 15 \text{ M}\Omega$) and the pyroelectric current (I) is estimated as $V = IR$. The pyroelectric coefficient (p) is calculated as

$$I = pA \frac{dT}{dt} \quad (10)$$

where dT/dt is the rate of temperature variation. It is to note that the estimated pyroelectric coefficient could be underestimated because the selected load resistance is not optimized for maximum electric current flow. Figure 5(a) shows the dT/dt rate of temperature variation, whereas Figure 6 shows the voltage (V) across the resistance ($R = 15 \text{ M}\Omega$); these data are used in conjunction with equation (10) and the estimated p value is $1 \times 10^{-4} \text{ C/m}^2 \text{ K}$ for the 15% cement composites. Similarly, the p values for pure BSZTO and the 20% cement composite are also estimated as $\sim 2.1 \times 10^{-4}$ and $\sim 0.8 \times 10^{-4} \text{ C/m}^2 \text{ K}$, respectively. Recently, we

have measured p for pure BSZTO as $3.4 \times 10^{-4} \text{ C/m}^2 \text{ K}$ (303 K) using the direct measurement method (Patel et al., 2018). The present method of p estimation is in good agreement with the direct measurement method of Patel et al. (2018). It can be expected that the p values for the other two compositions are also within the expected range. The pyroelectric coefficient (p), dielectric constant (ϵ_r), and loss ($\tan \delta$) can be utilized to determine the various pyroelectric FOMs. The details of pyroelectric FOMs (BSZTO) are discussed in the literature (Patel et al., 2018) and compared with the values reported in the literature. The FOM for voltage responsivity is expanded as $F_v = p/c_v \epsilon_r \epsilon_0$, high detectivity-based FOM is defined as $F_d = p/c_v \sqrt{\epsilon_r \epsilon_0} \tan \delta$, and energy harvesting-based FOMs as $F_e = p^2/\epsilon_r \epsilon_0$ and $F_e^* = p^2/c_v^2 \epsilon_r \epsilon_0$ used by various researchers for pyroelectric material selection (Patel et al., 2018; Srikanth et al., 2017, 2018). c_v is the specific heat capacity at a constant volume. These FOMs clearly indicated that, as ϵ_r decreases FOMs increase, and hence it is expected that the cement incorporation increases the FOM values up to 10 times than the FOMs for BSZTO ceramics. The same composition with glass incorporation already is detailedly discussed in a previous article (Srikanth et al., 2017). Similar behavior can also be observed in our case. Furthermore, Figure 6 presents the pyroelectric voltage (V_p) obtained using a non-switched circuit across 15 M Ω load resistance for the 15% cement composite which is in phase with temperature because the pyroelectric material is connected directly across load R_L and compare with the parallel SSHI technique. In addition, it is worth noting that the inversion of voltage of the material capacitance (switched voltage condition) as shown in Figure 7 for the 15% cement sample using the parallel SSHI technique depends on the inversion

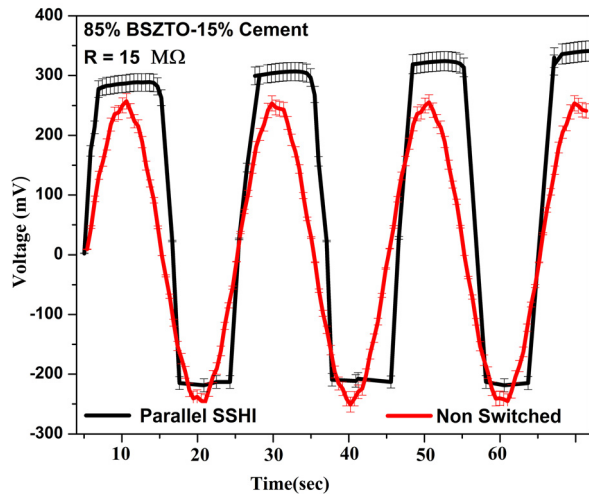


Figure 6. Voltage across 15 MΩ load resistance for the 15% cement composite employing for non-switched circuit and parallel SSHI.

factor γ because of switching of the circuit at its extreme temperature that leads to the oscillation of charges which results in a change in the waveform of

the pyroelectric material compared to the non-switched circuit. Similar patterns were observed for pure BSZTO and the 20% cement composition sample which are not shown here.

The pyroelectric element was further connected with a controlled switch and the effect of the switching process on the voltage signal of all the investigated compositions were used to compute the power across different load resistances and compared with non-switched power as shown in Figure 7. The output power of the pyroelectric generator strongly depends on the load resistance and it is maximum when load impedance is equal to source impedance in all the three cases of the 15% cement composite, 20% cement composite, and BSZTO ceramics. The optimum harvested power increased from 6 to 8.5 nW (using parallel switched interface) and 7.2 nW (using series switched interface) for the 15% cement specimen as shown in Figure 7(a). Similarly, the optimum harvested power obtained for the 20% cement sample is shown in Figure 7(b). The power obtained for series SSHI is less as compared to parallel SSHI due to the effect of load resistance which falls during the discharging loop when the switch is in

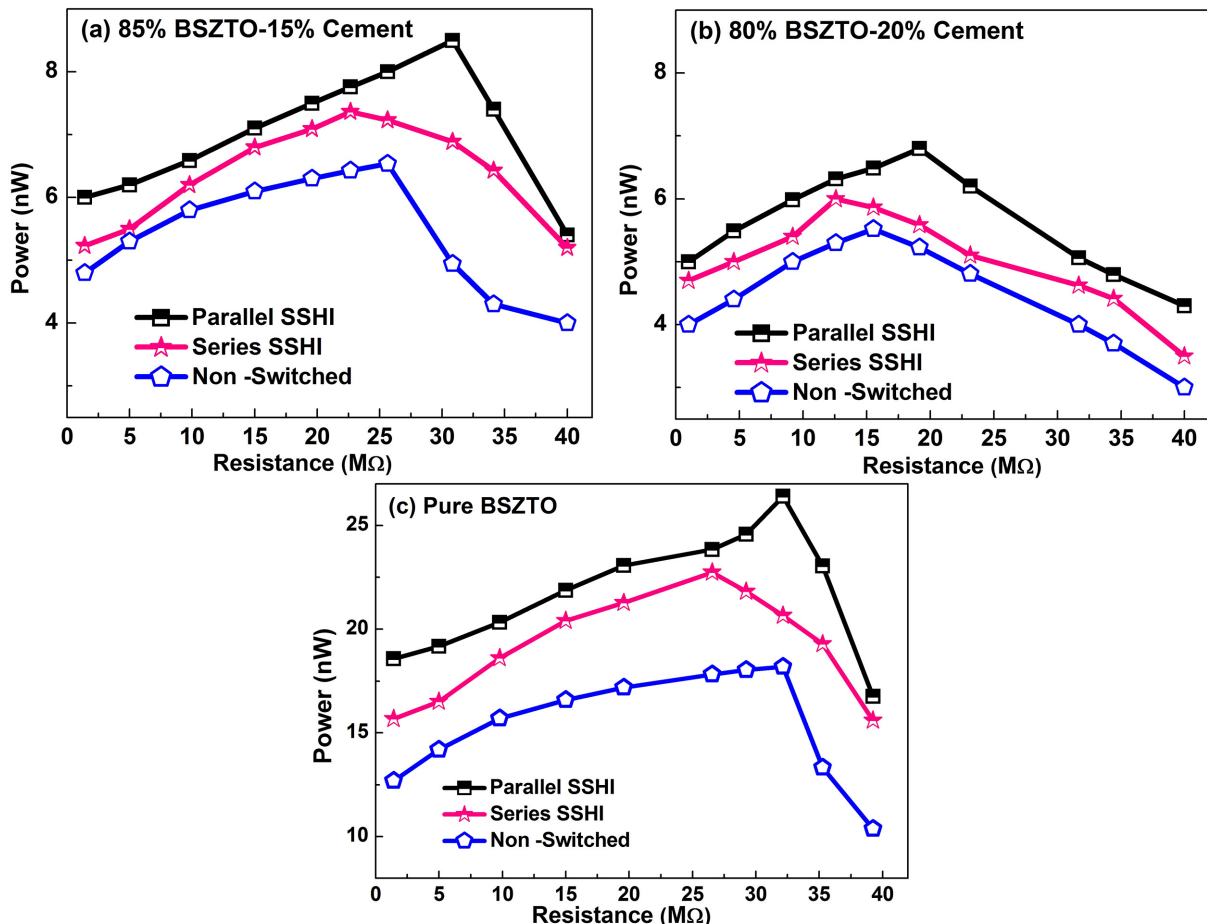


Figure 7. Harvested electrical power as a function of load resistance for (a) 15% cement composite, (b) 20% cement composite, and (c) BSZTO ceramics.

ON state which leads to poor voltage inversion compared to parallel SSHI. However, the power harvested from pure BSZTO increased from 17 to 27 nW (using parallel SSHI) and 23 nW (using series SSHI) as shown in Figure 7(c).

4. Conclusion

In this study, cement-binded BSZTO composites (15% and 20% cement by weight) were fabricated by the normal mixing and pressing method. The dielectric constant and loss for all the investigated samples were determined. The dielectric constant decreased drastically for the cement composites, which is desirable for pyroelectric applications. It is imperative to note here that the electrical signal (power) in the cement composites is significant when compared with pure BSZTO ceramics. Consequently, this trademark highlights the potential of cement-based materials for pyroelectric applications. A 4 μ H inductor with resistance (55 Ω) is used in the switched interface that leads to a quality factor (Q) of 6 for the 15% cement composite with C_p determined from the impedance analyzer at 45°C and the optimized power is found to be 7.2 and 6 nW in series SSHI and 8.5 and 7 nW in parallel SSHI for the 15% and 20% cement composites, respectively, which is sufficient for pyroelectric sensing applications. The results reveal that the non-linear processing technique based on SSHI leads to significant power improvement compared to non-switched interface.

Acknowledgements

R.V. acknowledges the support from the Indian National Science Academy (INSA), New Delhi, India through a grant by the Department of Science and Technology (DST), New Delhi, India under the INSA Young Scientists award.


Declaration of conflicting interests

The author(s) declared no potential conflicts of interest with respect to the research, authorship, and/or publication of this article.

Funding

The author(s) received no financial support for the research, authorship, and/or publication of this article.

ORCID iD

Rahul Vaish  <https://orcid.org/0000-0001-7510-7302>

References

Bauer S and Ploss B (1990) A method for the measurement of the thermal, dielectric, and pyroelectric properties of thin

- pyroelectric films and their applications for integrated heat sensors. *Journal of Applied Physics* 68(12): 6361–6367.
- Chen Y-Y, Vasic D, Costa F, et al. (2012) A self-powered switching circuit for piezoelectric energy harvesting with velocity control. *The European Physical Journal Applied Physics* 57(3): 30903.
- Cheng X, Miao L, Song Y, et al. (2017) High efficiency power management and charge boosting strategy for a triboelectric nanogenerator. *Nano Energy* 38: 438–446.
- Clegg WW, Jenkins DFL and Cunningham MJ (1997) The preparation of piezoceramic-polymer thick films and their application as micromechanical actuators. *Sensors and Actuators, A: Physical* 58(3): 173–177.
- Dietze M, Krause J, Solterbeck CH, et al. (2007) Thick film polymer-ceramic composites for pyroelectric applications. *Journal of Applied Physics* 101(5): 054113.
- Dong B, Liu Y, Qin L, et al. (2015) In situ stress monitoring of the concrete beam under static loading with cement-based piezoelectric sensors. *Nondestructive Testing and Evaluation* 30(4): 312–326.
- Furukawa T, Fujino K and Fukada E (1976) Electromechanical properties in the composites of epoxy resin and PZT ceramics. *Japanese Journal of Applied Physics* 15(11): 2119–2129.
- Gong H, Li Z, Zhang Y, et al. (2009) Piezoelectric and dielectric behavior of 0–3 cement-based composites mixed with carbon black. *Journal of the European Ceramic Society* 29(10): 2013–2019.
- Guyomar D and Lallart M (2011) Recent progress in piezoelectric conversion and energy harvesting using nonlinear electronic interfaces and issues in small scale implementation. *Micromachines* 2: 274–294.
- Guyomar D, Sebald G, Lefevre E, et al. (2008) Toward heat energy harvesting using pyroelectric material. *Journal of Intelligent Material Systems and Structures* 20(3): 265–271.
- Jayasundere N and Smith BV (1993) Dielectric constant for binary piezoelectric 0–3 composites. *Journal of Applied Physics* 73(5): 2462–2466.
- Lallart M (2017) Nonlinear technique and self-powered circuit for efficient piezoelectric energy harvesting under unloaded cases. *Energy Conversion and Management* 133: 444–457.
- Lang SB (2005) Pyroelectricity: from ancient curiosity to modern imaging tool. *Physics Today* 58(8): 31–36.
- Lang SB, Zhu WY and Cross LE (2006) Piezoelectric and pyroelectric properties of $(K_{0.5}Na_{0.5})(1-x)(Nb_{1-y}Ta_y)O_3$ ceramics. *Ferroelectrics* 336: 15–21.
- Lau ST, Cheng CH, Choy SH, et al. (2008) Lead-free ceramics for pyroelectric applications. *Journal of Applied Physics* 103(10): 104105.
- Lefevre E, Badel A, Richard C, et al. (2006) A comparison between several vibration-powered piezoelectric generators for standalone systems. *Sensors and Actuators, A: Physical* 126(2): 405–416.
- Lefevre E, Sebald G, Guyomar D, et al. (2009) Materials, structures and power interfaces for efficient piezoelectric energy harvesting. *Journal of Electroceramics* 22(1–3): 171–179.
- Li X, Lu S-G, Chen X-Z, et al. (2013) Pyroelectric and electrocaloric materials. *Journal of Materials Chemistry C* 1(1): 23–37.

- Li Z, Gong H and Zhang Y (2009) Fabrication and piezoelectricity of 0–3 cement based composite with nano-PZT powder. *Current Applied Physics* 9(3): 588–591.
- Lien IC, Shu YC, Wu WJ, et al. (2010) Revisit of series-SSHI with comparisons to other interfacing circuits in piezoelectric energy harvesting. *Smart Materials and Structures* 19(12): 125009:120521.
- Liu X, Chen Z, Wu D, et al. (2015) Enhancing pyroelectric properties of Li-doped $(\text{Ba}_{0.85}\text{Ca}_{0.15})(\text{Zr}_{0.1}\text{Ti}_{0.9})\text{O}_3$ lead-free ceramics by optimizing calcination temperature. *Japanese Journal of Applied Physics* 54: 071501.
- Lu Y, Ma H and Li Z (2015) Ultrasonic monitoring of the early-age hydration of mineral admixtures incorporated concrete using cement-based piezoelectric composite sensors. *Journal of Intelligent Material Systems and Structures* 26(3): 280–291.
- Patel S and Vaish R (2016) Effect of sintering temperature and dwell time dependent dynamic hysteresis scaling behavior of $(\text{Ba}_{0.85}\text{Ca}_{0.075}\text{Sr}_{0.075})(\text{Ti}_{0.90}\text{Zr}_{0.10})\text{O}_3$ ceramics. *Ferroelectrics* 505(1): 52–66.
- Patel S, Chauhan A and Vaish R (2015a) Electrocaloric behavior and temperature-dependent scaling of dynamic hysteresis of $\text{Ba}_{0.85}\text{Ca}_{0.15}\text{Ti}_{0.9}\text{Zr}_{0.1}\text{O}_3$ ceramics. *International Journal of Applied Ceramic Technology* 12(4): 899–907.
- Patel S, Chauhan A and Vaish R (2016) Large pyroelectric figure of merits for Sr-modified $\text{Ba}_{0.85}\text{Ca}_{0.15}\text{Zr}_{0.1}\text{Ti}_{0.9}\text{O}_3$ ceramics. *Solid State Sciences* 52: 10–18.
- Patel S, Chauhan A, Kundu S, et al. (2015b) Tuning of dielectric, pyroelectric and ferroelectric properties of $0.715\text{Bi}_{0.5}\text{Na}_{0.5}\text{TiO}_3 - 0.065\text{BaTiO}_3 - 0.22\text{SrTiO}_3$ ceramic by internal clamping. *AIP Advances* 5(8): 87145-87162.
- Patel S, Srikanth KS, Steiner S, et al. (2018) Pyroelectric and impedance studies of the $0.5 \text{Ba} (\text{Zr}_{0.2}\text{Ti}_{0.8}) \text{O}_3 - 0.5(\text{Ba}_{0.7}\text{Sr}_{0.3}) \text{TiO}_3$ ceramics. *Ceramics International* 44: 21976–21981.
- Roscow J, Zhang Y, Taylor J, et al. (2015) Porous ferroelectrics for energy harvesting applications. *The European Physical Journal: Special Topics* 224(14–15): 2949–2966.
- Sasaki A, Chiba T, Mamiya Y, et al. (1999) Dielectric and piezoelectric properties of $(\text{Bi}_{0.5}\text{Na}_{0.5})\text{TiO}_3 - (\text{Bi}_{0.5}\text{K}_{0.5})\text{TiO}_3$ systems. *Japanese Journal of Applied Physics* 38(Suppl. 9): 5564.
- Shaw CP, Whatmore RW and Alcock JR (2007) Porous, functionally gradient pyroelectric materials. *Journal of the American Ceramic Society* 90(1): 137–142.
- Shu YC, Lien IC and Wu WJ (2007) An improved analysis of the SSHI interface in piezoelectric energy harvesting. *Smart Materials and Structures* 16(6): 2253–2264.
- Srikanth KS, Patel S and Vaish R (2018) Functional cementitious composites for pyroelectric applications. *Journal of Electronic Materials* 47(4): 2378–2385.
- Srikanth KS, Patel S, Steiner S, et al. (2017) Engineered microstructure for tailoring the pyroelectric performance of $\text{Ba}_{0.85}\text{Sr}_{0.15}\text{Zr}_{0.1}\text{Ti}_{0.9}\text{O}_3$ ceramics by $3\text{BaO}-3\text{TiO}_2-\text{B}_2\text{O}_3$ glass addition. *Applied Physics Letters* 110(23): 232901.
- Sun R, Wang J, Wang F, et al. (2014) Pyroelectric properties of Mn-doped $94.6\text{Na}_{0.5}\text{Bi}_{0.5}\text{TiO}_3 - 5.4\text{BaTiO}_3$ lead-free single crystals. *Journal of Applied Physics* 115(7): 74101–74105.
- Wen S and Chung DDL (2003) Pyroelectric behavior of cement-based materials. *Cement and Concrete Research* 33(10): 1675–1679.
- Whatmore RW (1986) Pyroelectric devices and materials. *Reports on Progress in Physics* 49(12): 1335–1386.
- Wu L, Do XD, Lee SG, et al. (2017) A self-powered and optimal SSHI circuit integrated with an active rectifier for piezoelectric energy harvesting. *IEEE Transactions on Circuits and Systems I: Regular Papers* 64(3): 537–549.
- Xi F, Pang Y, Li W, et al. (2017) Universal power management strategy for triboelectric nanogenerator. *Nano Energy* 37: 168–176.
- Xin C, Shifeng H, Jun C, et al. (2007) Piezoelectric, dielectric, and ferroelectric properties of 0–3 ceramic/cement composites. *Journal of Applied Physics* 101(9): 94110.
- Yao S, Ren W, Ji H, et al. (2012) High pyroelectricity in lead-free $0.5\text{Ba}(\text{Zr}_{0.2}\text{Ti}_{0.8})\text{O}_3 - 0.5(\text{Ba}_{0.7}\text{Ca}_{0.3})\text{TiO}_3$ ceramics. *Journal of Physics D: Applied Physics* 45(19): 195301–195306.
- Yu P, Ji Y, Neumann N, et al. (2012) Application of single-crystalline PMN-PT and PIN-PMN-PT in high-performance pyroelectric detectors. *IEEE Transactions on Ultrasonics, Ferroelectrics, and Frequency Control* 59(9): 1983–1989.
- Zhang H, Jiang S and Kajiyoshi K (2009) Pyroelectric and dielectric properties of Mn modified $0.82\text{Bi}_{0.5}\text{Na}_{0.5}\text{TiO}_3 - 0.18\text{Bi}_{0.5}\text{K}_{0.5}\text{TiO}_3$ lead-free thick films. *Journal of the American Ceramic Society* 92(9): 2147–2150.
- Zhang H, Jiang S and Kajiyoshi K (2010) Enhanced pyroelectric and piezoelectric figure of merit of porous $\text{Bi}_{0.5}(\text{Na}_{0.82}\text{K}_{0.18})0.5\text{TiO}_3$ lead-free ferroelectric thick films. *Journal of the American Ceramic Society* 93(7): 1957–1964.
- Zhang Y, Wang G, Zeng T, et al. (2007) Electric field-dependent dielectric properties and high tunability of porous $\text{Ba}_{0.5}\text{Sr}_{0.5}\text{TiO}_3$ ceramics. *Journal of the American Ceramic Society* 90(4): 1327–1330.
- Zi Y, Wang J, Wang S, et al. (2016) Effective energy storage from a triboelectric nanogenerator. *Nature Communications* 7: 10987.